Int. J. Electrochem. Sci., 14 **(2019)** 5535 – 5546, doi: 10.20964/2019.06.70

International Journal of ELECTROCHEMICAL SCIENCE
www.electrochemsci.org

Hierarchical MoS_2 Nanosheets - $FeCo_2O_4$ Nanowires on Flexible Carbon Cloth Substrate for High-Performance Flexible Supercapacitors

Selvaraj Shanthi[1,2], Hiroya Ikeda[1], Indrajit M. Patil[3], Bhalchandra kakade[3], Yasuhiro Hayakawa[1], Suru Ponnusamy[2], Chellamuthu Muthamizhchelvan[2]*

[1] Research Institute of Electronics, Shizuoka University, Japan.
[2] Department of Physics and Nanotechnology, SRM Institute of Science and Technology, Kattankulathur, India.
[3] SRM Research Institute, SRM Institute of Science and Technology, Kattankulathur, India.
[*]E-mail: selvancm@gmail.com

Received: 17 February 2019 / *Accepted:* 9 April 2019 / *Published:* 10 May 2019

In this work, the hybrid binder-free supercapacitor electrode material of MoS_2 nanosheets - $FeCo_2O_4$ nanowires on flexible carbon cloth (CC) substrate was fabricated using two-step hydrothermal approach. Initially, $FeCo_2O_4$ nanowires were synthesized on flexible CC and subsequently, MoS_2 nanosheets were deposited on $FeCo_2O_4$ nanowires - CC to form hierarchical core-shell nanostructure of hybrid binder-free MoS_2 - $FeCo_2O_4$ - CC electrode for superior electrochemical performance. The fabricated electrodes were characterized by using X-ray Diffractometer (XRD) analysis, Field Emission - Scanning Electron Microscopy (FE-SEM), Raman Spectroscopy and X-ray Photoelectron Spectroscopy (XPS) analysis. Electrochemical measurements were investigated by using cyclic voltammetry (CV) analysis and electrochemical impedance spectroscopy (EIS) analysis. The hybrid electrode exhibited a superior electrochemical performance with the specific capacitance value of 952 F/g at the scan rate of 5 mV/s and encompass the opportunity of developing flexible energy storage devices with high power yield.

Keywords: binder-free flexible electrodes; hierarchical core-shell nanostructure; flexible carbon cloth substrate; Electrochemical performance

1. INTRODUCTION

Research interest on flexible energy storage devices including flexible supercapacitors has developed as novel generation technologies for various applications in the field of wearable and portable electronics [1-7]. Flexible electrodes are the necessary constituent for the development of flexible supercapacitors. However, the construction of flexible supercapacitor electrodes is the bottleneck in the application of flexible electronics and many researchers are focusing on the construction of these flexible

electrodes for superior electrochemical performance. Generally, supercapacitor electrode materials are classified into three categories namely electrochemical double layer capacitors (EDLC), pseudocapacitors and hybrid capacitors [8]. EDLC include carbon-based materials like activated carbon, carbon fibers, graphene etc., Recently, carbon cloth (CC) is considered as one of the interesting substrates in the supercapacitor electrode materials, due to good mechanical strength, high conductivity and excellent flexibility [9-12]. So far, the highly investigated redox pseudocapacitive electrode materials include transition metal oxides, metal sulfides and conducting polymers. The combination of EDLC and pseudocapacitor electrode materials are denoted as hybrid electrode materials.

On comparing the EDLC carbon-based materials, the performance of pseudocapacitive materials is limited by its lower conductivity and low electrolyte-accessible surface area [13]. Various approaches have been proposed for improving the electrochemical performance of pseudocapacitive materials including nano structuration, directly depositing on high surface area materials like carbon fibers, carbon nano tubes (CNTs), graphene and porous conductive substrates, as a hybrid binder-free electrode material [14-16]. The transition metal oxides (RuO_2, NiO, MnO_2), mixed transition metal oxides with unique porous structures (Co_3O_4, $CuCo_2O_4$, $ZnCo_2O_4$, $FeCo_2O_4$, $NiCo_2O_4$) and metal sulfides (CoS_2, MoS_2) are some of the promising electrode materials for supercapacitors [17-19].

In this paper, the hybrid binder-free supercapacitor electrode material of MoS_2 nanosheets - $FeCo_2O_4$ nanowires on flexible CC substrate was developed using two-step hydrothermal approach. Figure 1 depicts the fabrication process of the hybrid binder-free electrode material of MoS_2 nanosheets - $FeCo_2O_4$ nanowires on flexible CC substrate. Principally, the $FeCo_2O_4$ nanowires on CC substrate were obtained using a step -1 hydrothermal approach and later, the MoS_2 nanosheets were decorated on the surface of $FeCo_2O_4$ nanowires, using a step -2 hydrothermal approach and thus forming the hybrid binder-free electrode material of MoS_2 -$FeCo_2O_4$ - CC. The fabricated electrodes were characterized by XRD, FE-SEM, Raman Spectroscopy, and XPS analysis. Electrochemical measurements were examined using cyclic voltammetry (CV) and electrochemical impedance spectroscopy (EIS) analysis.

2. EXPERIMENTATION

2.1 Materials used

All the purchased chemicals were of analytical grade, which are used directly without any further purification. Iron nitrate hexahydrate [$Fe(NO_3)_2 \cdot 6H_2O$], Cobalt nitrate hexahydrate [$Co(NO_3)_2 \cdot 6H_2O$], Urea [$CO(NH_2)_2$], Ammonium fluoride [$(NH_4)F$], Sodium molybdate [$Na_2MoO_4.6H_2O$], and Thiourea [CH_4N_2S] were acquired from Wako Chemicals, Japan. Carbon cloth (CC) substrate was obtained from sainergy fuel cell India.

2.2 Materials Characterizations

The fabricated binder-free electrodes were characterized by using RINT-2200 X-ray diffractometer, (XRD, Rigaku, Japan, CuKα radiation, λ=1.54178 Å). FE-SEM analysis was performed

using FE-SEM, JSM 7001F, (JEOL, Japan). Raman spectroscopy analysis was measured by NRS-7100 with a laser excitation wavelength of 532 nm and spot size 1 µm. X-ray photoelectron spectroscopy (XPS) measurements were conducted on Shimadzu ESCA-3100.

2.3 Electrochemical analysis

The electrochemical measurements were carried out at room temperature, using electrochemical workstation (CHI 760E) with a three-electrode measurement set up. For the cyclic voltammetry (CV) analysis, the fabricated binder-free electrodes $FeCo_2O_4$ - CC and MoS_2 - $FeCo_2O_4$ - CC were used as the working electrodes. Ag/AgCl electrode and graphite rod were used as reference and counter electrodes in 0.1 M aqueous KOH electrolyte solution. The Electrochemical Impedance Spectroscopy (EIS) analysis was performed in the frequency range of 1 Hz to 100 kHz at 5 mV AC voltage.

2.4 Hydrothermal synthesis of $FeCo_2O_4$ Nanowires on flexible CC - Step 1

Initially, carbon cloth (CC: 2 cm x 2 cm) substrate was pre-cleaned with 3 M HCl solution for 15 min to annihilate the surface impurities and rinsed with DI water and ethanol for three times. In a typical hydrothermal synthesis procedure, 3 mmol of $Fe(NO_3)_2.6H_2O$, 6 mmol of $Co(NO_3)_2.6H_2O$, 10 mmol of NH_4F and 15 mmol of $Co(NH_2)_2$ were dissolved in 80 mL of DI water and stirred for 20 min to form the homogeneous mixture solution. The prepared homogeneous mixture solution was then shifted to a 100 mL Teflon lined stainless steel autoclave in addition with pre-cleaned CC substrate and maintained at 130 ˚C for 5 h for hydrothermal reactions. After cooling down to room temperature, the fabricated binder-free electrode material of $FeCo_2O_4$ - CC was rinsed with DI water and ethanol for several times and dried at 80 ˚C for overnight. Finally, the fabricated binder-free electrode material was calcined at 200 ˚C for 5 h in air.

2.5 Hydrothermal synthesis on the fabrication of hybrid electrode material of MoS_2 Nanostructures - $FeCo_2O_4$ Nanowires on CC - Step 2

In a typical hydrothermal synthesis procedure, 0.5 g of $Na_2MoO_4.6H_2O$ and 1.0 g of CH_4N_2S were dissolved in 80 mL of DI water and stirred for 20 min to form the homogeneous mixture. The fabricated binder-free electrode material of $FeCo_2O_4$ - CC (from step -1 hydrothermal approach) was also placed in the homogeneous mixture and transferred to a 100 mL Teflon lined stainless steel autoclave. The hydrothermal reaction process was maintained at 200 ˚C for 24 h and cooled down to room temperature. The fabricated hybrid electrode material of MoS_2 -$FeCo_2O_4$ - CC was rinsed with DI water and ethanol for several times and allowed to dry at 80 ˚C for overnight. Finally, the hybrid electrode material of MoS_2 -$FeCo_2O_4$ - CC was calcined at 200 ˚C for 5 h in air.

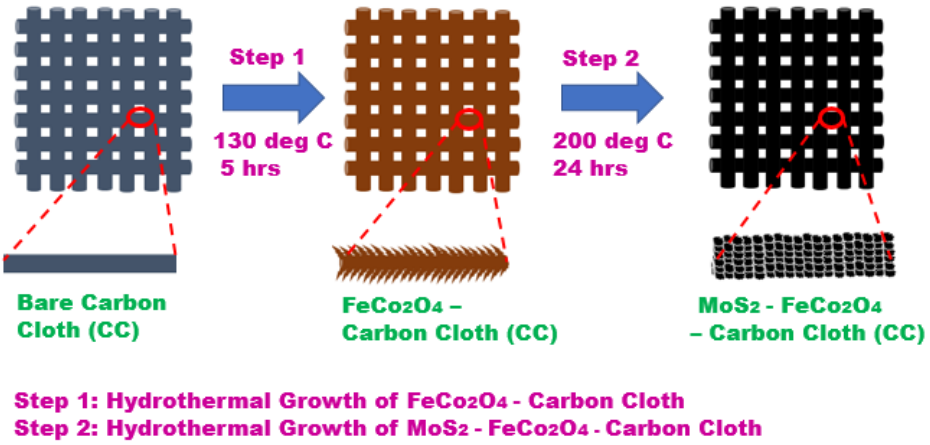

Figure 1. Schematic depiction of the fabrication process of the hybrid binder-free electrode material - MoS_2 nanosheets - $FeCo_2O_4$ nanowires on flexible CC substrate.

3. RESULTS AND DISCUSSION

Figure 2 displays the XRD profiles of $FeCo_2O_4$ - CC and MoS_2 - $FeCo_2O_4$ - CC. For the fabricated electrodes, the XRD peaks of CC substrate are clearly signified and well matched with the previous reports. From the XRD profile of fabricated electrode material of $FeCo_2O_4$ - CC, the obtained dominant diffraction crystal planes of (311) and (400) are accredited to a pure single - phase cubic spinel structure and a space group of Fd-3m is recognized with the JCPDS number of (04-0850) [20,21]. From the XRD profile of hybrid electrode material of MoS_2-$FeCo_2O_4$ - CC, the attained diffraction crystal planes of (002), (004) and (100) are attributed to the crystal plane of MoS_2 nanostructures (JCPDS No. 37-1492) [22].

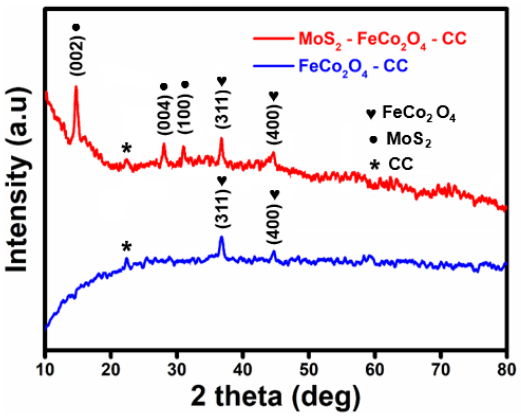

Figure 2. XRD profiles of $FeCo_2O_4$ - CC and MoS_2 - $FeCo_2O_4$ - CC.

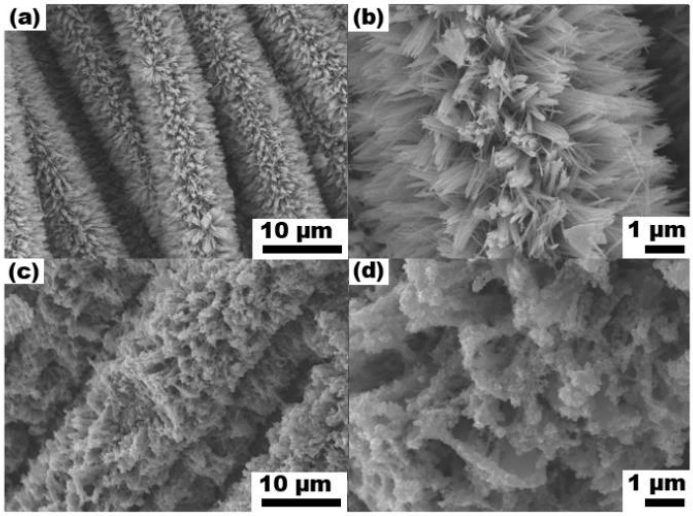

Figure 3. FE - SEM analysis of $FeCo_2O_4$ nanowires on CC (a, b) and MoS_2 nanosheets - $FeCo_2O_4$ nanowires on CC (c, d).

Figure 3 (a-d) represents the FE - SEM analysis of $FeCo_2O_4$ nanowires on CC and MoS_2 nanosheets - $FeCo_2O_4$ nanowires on CC. Figure 3a displays the low-magnification FE - SEM image of $FeCo_2O_4$ nanowires on CC, which clearly shows that the entire CC substrate is uniformly covered with dense $FeCo_2O_4$ nanowires. From Figure 3b, the high-magnification FE - SEM image of $FeCo_2O_4$ nanowires shows that the pointed structure of $FeCo_2O_4$ nanowires is obtained with an average diameter of ~100 nm and a length of ~5 μm. It is prophesied that the fabricated $FeCo_2O_4$ nanowires on CC have excellent capillary pathways along with good electron transportation capability, which is indispensable to enhance the electrochemical performance of the fabricated electrode materials due to the rapid insertion and extraction of electrolyte ions during the electrochemical process. As seen in the FE - SEM image of Figure 3c, it is obvious that the surface of $FeCo_2O_4$ nanowires was decked with a large number of MoS_2 nanosheets. From Figure 3d, the high magnification FE - SEM image divulges that the MoS_2 nanosheets are organized with each other, resulting in core-shell structure on flexible CC substrate. This kind of ordered construction of MoS_2 nanosheets on $FeCo_2O_4$ nanowires with copious open space is beneficial for the quick and easy access of electrolyte ions to the electrode/electrolyte interface, which results in lower ion - transport resistance and offer numerous active sites for redox reactions.

The reaction mechanism of $FeCo_2O_4$ nanowires includes a nucleation and subsequent growth process. At first, the precursor nanoparticles of $Fe_xCo_{2x}(OH)_{6x}$ were formed during the hydrothermal synthesis (step-1) of dissociation of Fe^{2+} and Co^{2+} ions with OH^- ions produced by the hydrolysis of urea ($Co(NH_2)_2$). The as-formed $Fe_xCo_{2x}(OH)_{6x}$ precursor nanoparticles may stick to the flexible CC substrate and stacked upon each other. And, driven by the minimization of surface energy, the organized precursor nanoparticles grew into $FeCo_2O_4$ nanowires in a privileged crystal orientation [23], through the succeeding annealing process. The fabricated $FeCo_2O_4$ nanowires on CC were served as a template, by providing a greater number of activation sites for the subsequent growth of MoS_2.

By the subsequent hydrothermal process (step-2) with the MoS_2 precursor solution of $Na_2MoO_4.6H_2O$ and CH_4N_2S, MoS_2 nanocrystals were formerly produced over the surface of $FeCo_2O_4$ nanowires on CC. These produced MoS_2 nanocrystals further grew into MoS_2 nanosheets over the

surface of $FeCo_2O_4$ nanowires on CC by the oriented attachment effect, which results in the formation of core-shell nanostructure of MoS_2 nanosheets - $FeCo_2O_4$ nanowires on CC. The formation mechanism of MoS_2 - $FeCo_2O_4$ on CC is estimated in the following equations [24-25]. The reaction mechanism of $FeCo_2O_4$ on CC substrate is given as,

$$Co(NH_2)_2 + H_2O \rightarrow C_3H_6N_6 + 6NH_3 + 3Co_2 \quad (1)$$

$$NH_3 + NH_4F + H_2O \rightarrow 2NH^{4+} + OH^- + F^- \quad (2)$$

$$xFe^{2+} + 2xCo^{2+} + 6xOH^- \rightarrow Fe_xCo_{2x}(OH)_{6x} \quad (3)$$

$$Fe_xCo_{2x}(OH)_{6x} + 0.5xO_2 \rightarrow xFeCo_2O_4 + 3xH_2O \quad (4)$$

And, the subsequent reaction mechanism of MoS_2 nanosheets over the surface of $FeCo_2O_4$ on CC is signified as,

$$SC(NH_2)_2 + 2H_2O \rightarrow Co_2 + 2NH_3 + H_2S \quad (5)$$

$$H_2S \rightarrow 2H^+ + S^{2-} \quad (6)$$

$$4\,MoO_4^{2-} + 9S^{2-} + 24H^+ \rightarrow 4\,MoS_2 + 12\,H_2O + SO_4^{2-} \quad (7)$$

Figure 4 signifies the Raman spectroscopy analysis of $FeCo_2O_4$ - CC and MoS_2 - $FeCo_2O_4$ - CC. For the fabricated electrodes, three notable Raman peaks obtained at 1345, 1579 and 2693 cm^{-1}, agreeing to the D (disordered), G (graphitic) and 2D bands of CC substrate [26]. For the fabricated electrode of $FeCo_2O_4$ - CC, three Raman characteristics peaks obtained at 296, 480, 610 and 683 cm^{-1}, are accredited to the F_{2g}, E_g, and A_{1g} vibrational modes of $FeCo_2O_4$ [27,28]. In the Raman spectra of MoS_2 - $FeCo_2O_4$ - CC, two characteristic peaks attained at 382.4 and 407.6 cm^{-1}, are recognized to the E^1_{2g} and A_{1g} vibrational modes of MoS_2, respectively [29].

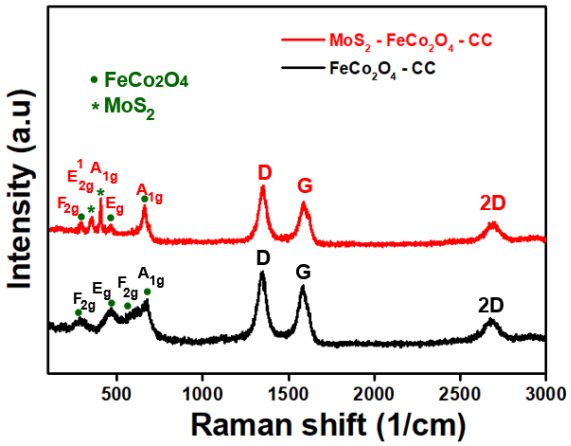

Figure 4. Raman spectroscopy analysis of $FeCo_2O_4$ - CC and MoS_2 - $FeCo_2O_4$ - CC.

Figure 5 represents the XPS spectra of the fabricated hybrid electrode material of MoS_2 -$FeCo_2O_4$ - CC. From Figure 5a, the Fe 2p electronic configurations accomplished at 712.3 and 727.1 eV, are assigned to Fe $2p_{3/2}$ and Fe $2p_{1/2}$ [30]. The electronic configuration of Co 2p identified at 780.8 (Co^{3+}) and 797.1(Co^{2+}) eV are allocated to Co $2p_{3/2}$ and Co $2p_{1/2}$, as revealed in Figure 5b [31, 32]. From Figure 5c, the carbon peak attained at 284.7 eV is allocated to C 1s spectra [33]. A strong peak observed at 162.2 eV is assigned to S 2p spectra, as shown in Figure 5d and the two peaks obtained at 232.6 and

228.5 eV, are ascribed to Mo $3d_{3/2}$ and Mo $3d_{5/2}$, as shown in Figure 5e [34]. The O 1s spectrum is achieved at 531.8 eV, as exposed in Figure 5f [35].

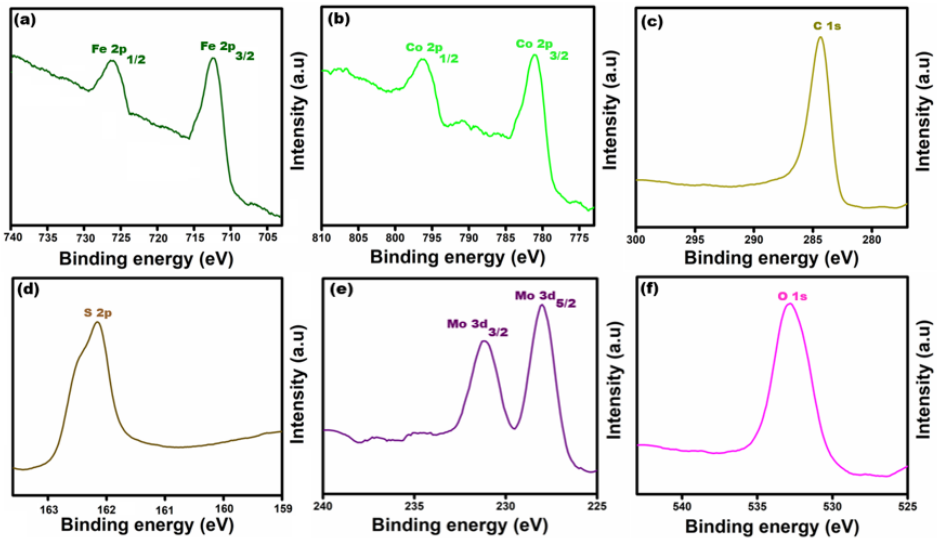

Figure 5. XPS spectra of the fabricated hybrid electrode material of MoS_2 -$FeCo_2O_4$ - CC. (a) Fe 2p, (b) Co 2p, (c) C 1s, (d) S 2p, (e) Mo 3d, and (f) O 1s.

Figure 6a represents the cyclic voltammetry (CV) curves of $FeCo_2O_4$ - CC electrode material using 0.1 M KOH as an electrolyte with the potential window of -0.25 V to +0.25 V. With the aid of OH^- anions, CV curves of $FeCo_2O_4$ - CC reproduces the reversible transitions of Co^{3+}/Co^{4+} and Fe^{2+}/Fe^{3+}. The conceivable redox reaction mechanism of $FeCo_2O_4$ - CC is embodied as below [36-38],

$$FeCo_2O_4 + H_2O + e^- \leftrightarrow 2CoOOH + Fe(OH)^- \quad (8)$$

$$CoOOH + OH^- \leftrightarrow CoO_2 + H_2O + e^- \quad (9)$$

$$FeOH + OH^- \leftrightarrow Fe(OH)_2 + e^- \quad (10)$$

The $FeCo_2O_4$ incorporated CC electrode material achieved faster electron transportation rate by successfully bridging the $FeCo_2O_4$ nanowires and reducing the interface resistance between the $FeCo_2O_4$ nanostructures and the CC substrate. Noticeably, with the increasing scan rate, the CV curve areas are also increased in its shape, which is due to the polarization effect of the fabricated electrode.

Figure 6b indicates the CV curves of the hybrid electrode material of MoS_2 - $FeCo_2O_4$ - CC with the same potential window. CV curves of MoS_2 - $FeCo_2O_4$ - CC exhibit the quasi-rectangular shapes, which indicates the presence of dual behavior of Electro chemical double layer capacitor (EDLC) and pseudo capacitive nature of the hybrid electrode [39, 40]. Additionally, no redox peaks were detected in the CV curves of hybrid electrode MoS_2 - $FeCo_2O_4$ - CC, which may be due to the formation of an electrical double layer at the electrode/electrolyte interface. It occurred due to the insertion/de-insertion of alkali ions (K^+) from the KOH electrolyte solution, during the electrochemical analysis of hybrid electrode MoS_2 - $FeCo_2O_4$ - CC.

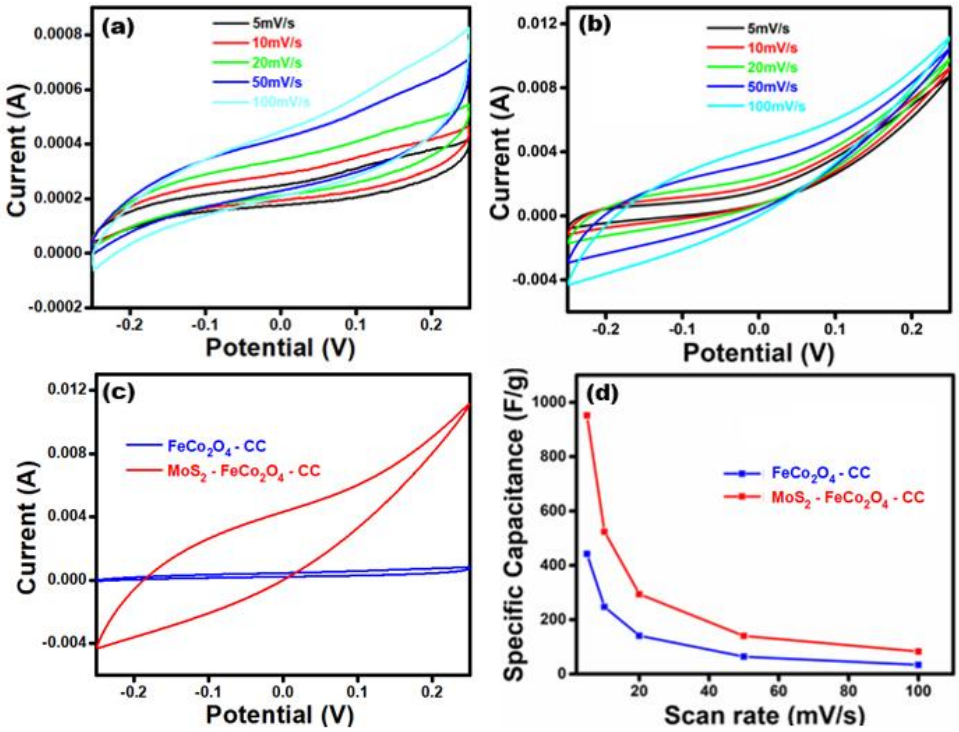

Figure 6. Cyclic Voltammetry (CV) plots of (a) $FeCo_2O_4$ - CC and (b) MoS_2 - $FeCo_2O_4$ -CC at various scan rates ranging from 5 to 100 mV/s. (c) Comparison CV plots of $FeCo_2O_4$ - CC and MoS_2 - $FeCo_2O_4$ - CC at the scan rate of 100 mV/s. (d) The relationship between specific capacitance and scan rate for $FeCo_2O_4$ - CC and MoS_2 - $FeCo_2O_4$ - CC.

Conferring to the literature, the alkali metal ions may diffuse into the surface of MoS_2 layer during the electrochemical analysis and is given as,

$$(MoS_2)_{surface} + K^+ + e^- \leftrightarrow (MoS_2 + K^+)_{surface} + e^- \quad (11)$$

With respect to the reversible reactions of Mo^{3+}/Mo^{2+} associated with the OH^- ions, a rectangular shaped CV curve is achieved with slight variations in the hybrid electrode MoS_2 - $FeCo_2O_4$ - CC. The possible redox reaction mechanism of hybrid electrode MoS_2 - $FeCo_2O_4$ - CC during the electrochemical analysis is denoted as below,

$$MoS_2 + OH^- \leftrightarrow MoSOH + e^- \quad (12)$$

$$MoSOH + OH^- \leftrightarrow MoSO + H_2O + e^- \quad (13)$$

Figure 6c presents the comparison CV curves of $FeCo_2O_4$ - CC and MoS_2 - $FeCo_2O_4$ - CC hybrid electrode material at the scan rate of 100 mV/s. It is clearly seen that the CV curve of MoS_2 - $FeCo_2O_4$ - CC is larger than the $FeCo_2O_4$ - CC, due to the synergistic effect which attained among the fabricated electrode materials during the electrochemical analysis [41]. Also, this proved that the hybrid electrode MoS_2 - $FeCo_2O_4$ - CC attained the superior electrochemical performance than the $FeCo_2O_4$ - CC electrode. Based on the CV curves, the specific capacitance can be measured by using the following equation, [42]:

$$C=Q/m\ (\Delta V) \quad (14)$$

Where, C(F/g) is the specific capacitance, Q(C) is the charge, m(g) is mass of the active material and ΔV(V) is the potential window. Figure 6d portrays the relationship between the specific capacitance

and scan rate for the fabricated electrode materials $FeCo_2O_4$ - CC and MoS_2 - $FeCo_2O_4$ - CC at different scan rates. The achieved specific capacitance values of the fabricated electrode $FeCo_2O_4$ - CC are 442, 247, 141, 64 and 34 F/g at the scan rate of 5, 10, 20, 50 and 100 mV/s. And, the fabricated hybrid electrode MoS_2 - $FeCo_2O_4$ -CC attained the specific capacitance values of 952, 524, 294, 140 and 83 F/g, for the same scan rate values. Hence, it is clearly seen that the hybrid electrode material of MoS_2 - $FeCo_2O_4$ - CC achieved the maximum specific capacitance of 952 F/g and the $FeCo_2O_4$ - CC electrode displayed the maximum specific capacitance value of 442 F/g, for the same scan rate value of 5 mV/s. As shown in Table 1, the electrochemical performance of the MoS_2 - $FeCo_2O_4$ - CC electrode is compared with other reported electrodes.

Table 1. Comparison of the electrochemical performance of the MoS_2 - $FeCo_2O_4$ - CC electrode with reported electrodes

Samples	Electrolyte used	Potential window	Capacitance	Ref.
$CuCo_2O_4$ - Ni Foam	KOH	0.0 - 0.5 V	820 F/g at 2 mA/cm^2	[14]
Natural graphite flakes: Perchloric Acid: Copper Nitrate: Potassium Permanganate - EG4	Na_2SO_4	−0.3 - 0.8 V	335.9 F/g at 0.5 A/g	[15]
Hierarchical Porous Carbon Nanorods (HPCRs)	KOH	−1.0 - 0.0 V	274 F/g at 0.5 A/g	[16]
$FeCo_2O_4$@MnO_2@Carbon Fibers	KOH	0.0 - 0.5 V	4.8 F/cm^2 at 1 mA/cm^2	[18]
MoS_2@Co_3O_4@Carbon Fibers	KOH	0.0 - 0.6 V	69 mAh/g at 0.5 A/g	[19]
MoS_2 - $FeCo_2O_4$ - CC	KOH	−0.25 - 0.25 V	952 F/g at 5 mV/s	This work

Figure 7 defines the EIS analysis of Bode plot for the fabricated electrode materials, (a) $FeCo_2O_4$ - CC and (b) MoS_2 - $FeCo_2O_4$ - CC. From Figure 7a and Figure 7b, at 1 Hz frequency, the achieved phase angles (from the data) of fabricated electrodes $FeCo_2O_4$ - CC and MoS_2 - $FeCo_2O_4$ - CC are denoted as -46.9° and -20.8°, respectively. This larger shift values in the phase angles of the fabricated electrode materials are likely due to the charge transfer mechanism of active materials with dissimilar components. Figure 7c shows the comparison Nyquist plot of fabricated electrodes and the obtained equivalent series resistance (ESR) values (from the data) of $FeCo_2O_4$ - CC and MoS_2 - $FeCo_2O_4$ - CC are signified as 0.9 Ω and 0.1 Ω, respectively.

The fabricated hybrid electrode material of MoS_2 - $FeCo_2O_4$ - CC exposed lower ESR values than the electrode $FeCo_2O_4$ - CC, which may likely due to the combination of EDLC and pseudocapacitive active materials in the hybrid electrode of MoS_2 - $FeCo_2O_4$ - CC. This lower ESR values of the fabricated electrode can integrate the design of supercapacitors with high power applications [43-45]. Additionally, at the high-frequency region of the fabricated electrodes of $FeCo_2O_4$

- CC and MoS_2 - $FeCo_2O_4$ - CC, no notable semicircle region is obtained, which clarifies the accomplishment of low faradaic resistances in the KOH electrolyte [46-47].

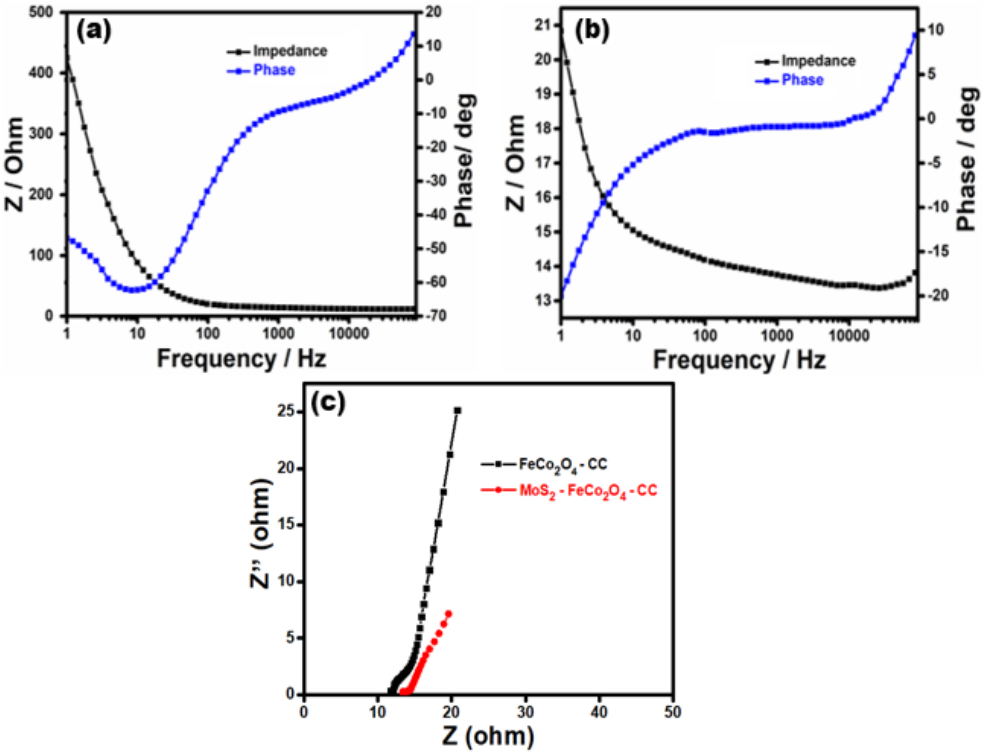

Figure 7. Electrochemical Impedance Spectroscopy (EIS) analysis - Bode plot of (a) $FeCo_2O_4$ - CC, (b) MoS_2 - $FeCo_2O_4$ - CC. (c) Nyquist plot of $FeCo_2O_4$ - CC and MoS_2 - $FeCo_2O_4$ - CC.

4. CONCLUSION

In summary, the hybrid binder-free supercapacitor electrode material of MoS_2 nanosheets - $FeCo_2O_4$ nanowires on flexible CC was successfully fabricated using two-step hydrothermal approach. XRD analysis confirmed the formation of core-shell nanostructure of MoS_2 - $FeCo_2O_4$ on flexible CC substrate and FE - SEM analysis exposed the homogeneity of $FeCo_2O_4$ nanowires on CC decorated with MoS_2 nanosheets. Raman spectroscopy analysis contented the vibrational modes of $FeCo_2O_4$, MoS_2, and CC with strong Raman characteristics peaks. XPS analysis clarified the electronic configurations of Fe 2p, Co 2p, O 1s, Mo 3d, S 2p and C 1s spectra for the fabricated hybrid binder-free electrode material MoS_2 - $FeCo_2O_4$ - CC. The electrochemical analysis was performed and the fabricated hybrid electrode material of MoS_2 - $FeCo_2O_4$ - CC displayed the maximum specific capacitance of 952 F/g and the $FeCo_2O_4$ - CC electrode exhibited the specific capacitance value of 442 F/g for scan rate value of 5 mV/s. Moreover, the hybrid binder-free electrode material MoS_2 - $FeCo_2O_4$ - CC displayed the lowest ESR value, which revealed the possibility of utilizing the above electrode for high power applications.

ACKNOWLEDGEMENTS
Financial assistance received from Shizuoka University, Japan is greatly acknowledged. We also thank the support from Japanese Government MONBUKAGAKUSHO: MEXT Scholarship.

References

1. L. Dong, C. Xu, Y. Li, Z. H. Huang, F. Kang, Q. H. Yang and X. Zhao, *J. Mater. Chem. A*, 4(13) (2016) 4659.
2. Y. Huang, H. Li, Z. Wang, M. Zhu, Z. Pei, Q. Xue, Y. Huang and C. Zhi, *Nano Energy*, 22 (2016) 422.
3. J. Chen, K. Fang, Q. Chen, J. Xu and C. P. Wong, *Nano Energy*, 53 (2018) 337.
4. L. Liu, Z. Niu and J. Chen, *Chinese Chem. Lett.*, 29 (2018) 571.
5. Y. Han, Y. Ge, Y. Chao, C. Wang and G. G. Wallace, *J. Energy Chem.*, 27 (2018) 57.
6. H. Luo, H. Lu and J. Qiu, *J. Electroanalytical Chem.*, 828 (2018) 24.
7. L. Liu, Y. Feng and W. Wu, *J. Pow. Sou.,* 410 (2019) 69.
8. H. Choi and H. Yoon, *Nanomaterials*, 5 (2015) 906.
9. L. Feng, G. Li, S. Zhang and Y. X. Zhang, *Ceramics Intl.,* 43(11) (2017) 8321.
10. T. Qin, S. Peng, J. Hao, Y. Wen, Z. Wang, X. Wang, D. He, J. Zhang, J. Hou and G. Cao, *Adv. Energy Mater.,* 7(20) (2017) 1700409.
11. Y. Zhang, Z. Hu, Y. Liang, Y. Yang, N. An, Z. Li and H. Wu, *J. Mater. Chem. A*, 3 (2015) 15057.
12. Y. Wang, S. Tang, S. Vongehr, J. A. Syed, X. Wang and X. Meng, *Scientific Rep.,* 6 (2016) 12883.
13. K. Makgopa, P. M. Ejikeme, C. J. Jafta, K. Raju, M. Zeiger, V. Presser and K. I. Ozoemena, *J. Mater. Chem. A*, 3 (2015) 3480.
14. Y. Wang, D. Yang, J. Lian, T. Wei and Y. Sun, *J. Alloy. and Comp.*, 741 (2018) 527.
15. N. Sykam, M. Ghosh and G. M. Rao, *J. Alloy. Comp.*, 769 (2018) 274.
16. L. Fang, Y. Xie, Y. Wang, Z. Zhang, P. Liu, N. Cheng, J. Liu, Y. Tu, H. Zhao and J. Zhang, *App. Surf. Sci.,* 464 (2019) 479.
17. S. Vijayakumar, S. Nagamuthu, S. H. Lee and K. S. Ryu, *Intl. J. Hydrogen Energy*, 42 (2017) 3122.
18. F. Zhu, Y. Liu, M. Yan and W. Shi, *J. Colloid. Interface Sci.*, 512 (2018) 419.
19. D. Liang, Z. Tian, J. Liu, Y. Ye, S. Wu, Y. Cai and C. Liang, *Electrochimica Acta,* 182 (2015) 376.
20. T. A. S. Ferreira, J. C. Waerenborgh, M. H. R. M. Mendonça, M. R. Nunes and F. M. Costa, *Sol. Stat. Sci.,* 5 (2003) 383.
21. S. G. Mohamed, C. Chen, C. K. Chen, S. Hu and R. Liu, *ACS Appl. Mater. Interf.,* 6 (2014) 22701.
22. S. V. P. Vattikuti, and C. Byon, *J. Nanomater.,* 2015 (2015) 1.
23. S. Liu, S. C. Lee, U. Patil, I. Shackery, S. Kang, K. Zhang, J. H. Park, K. Y. Chung and S. C. Jun, *J. Mater. Chem. A*, 5 (2017) 1043.
24. L. Shen, Q. Che, H. Li and X. Zhang, *Adv. Funct. Mater.,* 24(18) (2013) 2630.
25. G. Feng, A. Wei, Y. Zhao and J. Liu, *J. Mater. Sci.: Mater. Elect.,* 26(10) (2015) 8160.
26. F. Rosenburg, E. Ionescu, N. Nicoloso and R. Riedel, *Mater.,*11(1) (2018) 93.
27. V. Venkatachalam, A. Alsalme, A. Alghamdi and R. Jayavel, *J. Electroanalytical Chem.,* 756 (2015) 94.
28. K. K. Senapati, C. Borgohain and P. Phukan, *Catal. Sci. Technol.,* 2 (2012) 2361.
29. Y. Zhou, G. Liu, X. Zhu and Y. Guo, *Sens. Act. B Chem.,* 251 (2017) 280.
30. R. Liang, L. Shen, F. Jing, N. Qin and L. Wu, *ACS Appl. Mater. Interf.,* 7 (2015) 9507.
31. N. Wu, J. Low, T. Liu, J. Yu and S. Cao, *App. Surf. Sci.,* 413 (2017) 35.
32. J. Huang, D. Hou, Y. Zhou, W. Zhou, G. Li, Z. Tang, L. Li and S. Chen, *J. Mater. Chem. A,* 3 (2015) 22886.
33. P. Niedzialkowski, T. Ossowski, P. Zieba, A. Cirocka, P. Rochowski, S. J. Pogorzelski, J. Ryl, M. Sobaszek and R. Bogdanowicz, *J. Electroanalytical Chem.,* 756 (2015) 84.
34. J. Dolinska, A. Chidambaram, W. Adamkiewicz, M. Estili, W. Lisowski, M. Iwan, B. Palys, E. J. R. Sudholter, F. Marken, M. Opallo and L. J. Rassaei, *Mater. Chem. B*, 4 (2016) 1448.
35. Y. C. G. Kwan, G. M. Ng and C. H. A. Huan, *Thin Sol. Film.,* 590 (2015) 40.
36. S. Gao, F. Liao, S. Ma, L. Zhu and M. Shao, *J. Mater. Chem. A*, 3 (2015) 16520.
37. Q. Wang, D. Chen and D. Zhang, *RSC Adv.*, 5 (2015) 96448.

38. Q. Wang, X. Wang, J. Xu, X. Ouyang, X. Hou, D. Chen, R. Wang and G. Shen, *Nano Energy*, 8 (2014) 44.
39. Q. Cheng, J. Tang, J. Ma, H. Zhang, N. Shinya and L. C. Qin, *Carbon*, 49 (2011) 2917.
40. J. S. M. Lee, M. E. Briggs, C. C. Hu and A. I. Cooper, *Nano Energy*, 46 (2018) 277.
41. X. Chen, K. Yu, Y. Shen, Y. Feng and Z. Zhu, *ACS Appl. Mater. Interfaces,* 9 (48) (2017) 42139.
42. C. Wan, L. Yuan and H. Shen, *Int. J. Electrochem. Sci.,* 9 (2014) 4024.
43. A. S. Arico, P. Bruce, B. Scrosati, J. M. Tarascon and W. V. Schalkwijk, *Nat. Mater*., 4 (2005) 366.
44. E. Frackowiak and F. Beguin, *Carbon*, 39(6) (2001) 937.
45. J. Wang, S. Q. Zhang, Y. Z. Guo, J. Shen, S. M. Attia, B. Zhou, G. Z. Zheng and Y. S. Gui, *J. Electrochem. Soc.,* 148(6) (2001) D75.
46. Q. Wu, Y. Xu, Z. Yao, A. Liu and G. Shi, *ACS Nano*, 4 (2010) 1963.
47. H. Yin, J. Zhu, J. Chen, J. Gong and Q. Nie, *J. Mater. Sci.,* 53(17) (2018) 11951.